Energy transfer from rare gases to surfaces: Collisions with gold and platinum in the range 1–4000 eV

Harold F. Winters, H. Coufal, C. T. Rettner, and D. S. Bethune
IBM Research Division, 650 Harry Road, Almaden Research Center, San Jose, California 95120-6099
(Received 26 June 1989)

We have measured the energy transferred to a gold surface by impinging He^+, Ar^+, and Xe^+ ions with kinetic energies in the range 5–4000 eV. This same quantity has been determined for He, Ar, and Xe atoms colliding with a Pt(111) surface. The ion studies employed a novel highly sensitive pyroelectric calorimeter together with a carefully designed compact ion gun. Pulses of nearly monoenergetic ions from the gun were directed at a gold film evaporated directly onto a pyroelectric material that develops a voltage proportional to the energy deposited. The atomic studies were made with supersonic beam techniques, whereby energy transfer is inferred from time-of-flight distributions of the incident and scattered species. The results from these very different experiments are in good agreement and give a fairly complete picture of energy transfer from incident rare-gas atoms and ions to these heavy-metal surfaces. For energies above about 10 eV, the ions transfer at least 60% of their energy, with Xe transferring the most and He the least. For lower incident energies, the energy transfer decreases, approaching zero-energy intercepts of ~60%, 20%, and 5% for Xe, Ar, and He, respectively. The implications of these experimental results for the effective-mass concept, the binary-collision model, low-energy stopping powers, lattice penetration, and the theory of physical sputtering are considered, and we address the relevance of these findings to the technologically important processes of plasma etching and deposition of sputtered thin films and to particle-spacecraft interactions and controlled thermonuclear fusion.

I. INTRODUCTION

Knowledge of the amount of energy that an incoming atom or ion transfers to a surface during a collision is essential for the accurate modeling of many technologically important processes, including sputtering, plasma etching, and ion implantation. It is also crucial to the estimation of the drag on spacecraft[1,2] and to the design of thermonuclear fusion reactors. In the latter case, for example, energy losses from the plasma to the reactor walls have important consequences for the particle and energy balance of the system.[3]

The efficiency of energy transfer can be described quantitatively in terms of the energy reflection coefficient, $R(E_i)$, the mean value of the fraction of the incident energy E_i reflected from the surface, or equivalently, in terms of the energy deposition coefficient, $f(E_i) \equiv 1-R(E_i)$. This quantity is expected to be a function of the mass, kinetic energy and angle of the incident species, as well as the mass of the substrate atoms and possibly the surface morphology. Theoretical expressions and phenomenological descriptions for $R(E_i)$ remain untested because of an almost complete absence of relevant experimental measurements below a few keV. In part this is because of the considerable experimental difficulties associated with these measurements, particularly at low energies.

In this paper we report the first results of a systematic study of energy deposition from singly charged rare-gas ions to surfaces. We have employed a novel pyroelectric calorimeter to measure the energy deposition coefficient, $f(E_i)$, for He, Ar, and Xe ions striking a gold surface with energies in the range 5–4000 eV. These measurements have been supplemented for energies below 15 eV by supersonic atomic-beam measurements of the energy that neutral He, Ar, and Xe atoms lose in collisions with the similar Pt(111) surface. Taken together, these measurements describe rare-gas energy loss to heavy-metal surfaces for collision energies ranging from 4000 eV down to essentially zero.

While there have been a number of previous studies of energy deposition for ions with energies above 3500 eV,[4–9] and a range of theoretical calculations and simulations,[10–13] we believe that this is the first reliable experimental study for lower incidence energies. Early work by Winters[14] was difficult to interpret as measurements were made with a poorly defined incidence angle. Similarly, the results of Gesang, *et al.*[15] were taken in a somewhat ill-defined plasma environment where accurate current measurements are difficult to make. Eckstein and Verbeek[16] and Sorensen[17] have published some results for energies down to 1500 eV, but these are restricted to the case of protons.

Sections II A and II B of this paper describe the experiments conducted with ions and atomic beams, respectively. Sections III A and III B give the corresponding experimental results, which are compared to each other in Sec. III C. Sections IV A–IV G discuss some implications of these results for binary collision models, sticking probabilities, lattice penetration, physical sputtering, plasma etching, sputtered thin films, and particle-spacecraft interactions and controlled thermonuclear fusion. Section

V gives a summary of the results and some conclusions.

To give a brief overview of our results, we find that for incident kinetic energies above about 10 ev, all of the ions transfer at least 60% of their energy, with Xe transferring the most and He the least. For lower incident energies, using the atomic-beam method, we find that the energy transfer from Xe remains above 60% as the collision energy approaches zero, while for Ar and He collisions with the surface become increasingly elastic, with less than 20% and 5% energy transfer, respectively, in the low-energy limit.

II. EXPERIMENTAL

A. Ion-beam experiments

The relevant experiments are conceptually simple. We wish to measure the fraction of the kinetic energy of an incident ion that is deposited in a solid. This requires preparation of ions of a known energy that can be directed at a target surface, and the quantitative detection of the amount of energy deposited and the number of ions striking the surface. In practice, such measurements must overcome space-charge limitations on beam flux, which demands careful experimental design as well as a sensitive detection method. Our approach has been to combine a highly sensitive calorimeter with a novel ion gun.

1. Pyroelectric calorimeter

Energy deposition measurements are made with a specially built pyroelectric calorimeter, which is displayed schematically in Fig. 1, and that has been described in detail elsewhere.[18] The principle behind this device is that an output voltage is generated at the back surface of the calorimeter in proportion to the temperature of a pyroelectric film, which rises in response to energy deposition. For the purpose of these measurements a gold film is deposited directly onto the front surface of a pyroelectric film, which is then grounded and masked by a 3.2-mm aperture through which ion bombardment occurs. The sensitivity of this device is such that adequate signal-to-noise ratios can be obtained with a beam intensity of 1 μA/cm^2 (corresponding to a total incident current of $\sim$80 nA).

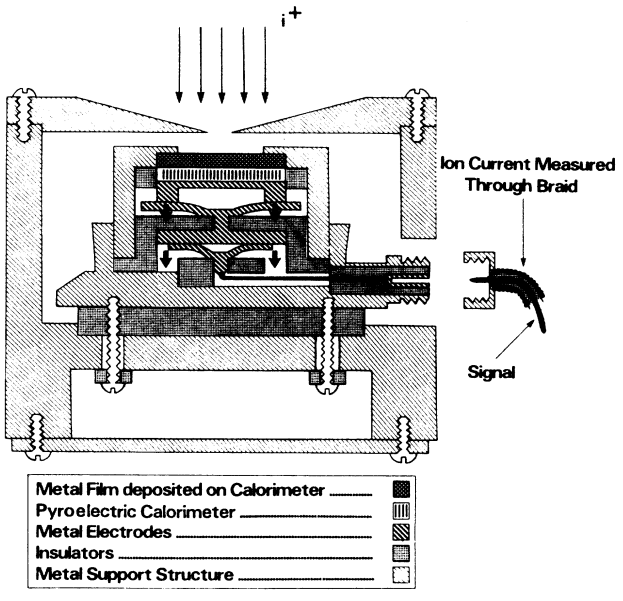

FIG. 1. Pyroelectric calorimeter. The modulated-ion beams bombard the grounded front surface of the calorimeter through a 3.2-mm-diam aperture. The signal goes from the back electrode through two spring contacts (indicated by arrows) to a lockin detector.

2. Ion-beam generation

To generate monoenergetic ion beams of this intensity down to a few eV required the development of a compact ion gun designed to minimize energy dispersion. Its principle of operation is rather unusual and will therefore be described in some detail. The general layout is shown in Fig. 2. Electrons are accelerated from the cathode into a virtually field-free region defined by electrodes *F*, *E*, *D*, and *C*, where they generate ions as a consequence of electron-atom collisions. Typical potentials for all electrodes with respect to the filament are given in the figure caption. The electrons are decelerated and reversed in direction in the region between electrodes *B* and *C*. The electron beam is concentrated and maintained on the center axis of the tube by a coaxial magnetic field. Most of the ions exit the end of the tube away from the cathode for the following reasons: First, the ions are forced away from the cathode by an electric field between electrodes *G* and *F*, and second, the ions are prevented from going radially to the wall by the line charge associated with the electron beam. Therefore, they leave through electrode *C*, are accelerated by *B*, focused by *A*, and collide with the grounded front surface of the calorimeter. We estimate, using known ionization cross sections and the geometrical path length, that most of the ions generated in the field-free region are eventually collected by the calorimeter. This is supported by measurements made with a Faraday cup detector in place of the calorimeter.

The ion energy remains well-defined because nearly all of the ions are generated and extracted from a field-free region. The ions are all singly charged because the electron energy is maintained below the level that would be needed to generate the doubly charged species. This has been experimentally verified by focusing the beam into a quadrupole mass spectrometer, which showed no appreciable intensity in peaks due to doubly charged ions. Sufficiently large currents are obtained because of the large collection efficiency and because the small distances minimize space-charge problems. The gun is typically operated with an internal noble-gas pressure of 1×10^{-5} Torr in a vacuum system where the base pressure is in the low 10^{-10} Torr region. These operating conditions eliminate charge exchange and impurity ions as problems.

During a typical set of runs the ion current to the sample is held constant by controlling the electron-beam extraction potential on electrode *G* and the ion focusing potential on electrode *A*. The potentials with respect to the

filament of all other electrodes are held constant. The ion energy is controlled by biasing the entire gun with respect to ground, so that the cylinder E is at V_i with respect to ground. The beam is chopped by application of a square wave to electrode G, which gates the electron beam.

Figure 3 shows the ion current to the calorimeter as a function of the bias voltage, V_i, the potential difference between the (grounded) front surface of the calorimeter and the field-free region where the ions are generated. The curve shows that the ions have enough energy to reach the calorimeter when this potential difference is positive and not enough when it is negative. This is, in fact, a retarding potential curve, and one can immediately see that the ion current drop is centered at $V_i=0$, so that the mean ion energy in eV will be given quite accurately by the applied potential, V_i, and also that the energy spread of the ions is not more than ± 1.5 eV. Note that nearly the full current of the gun is still obtained at 3 eV.

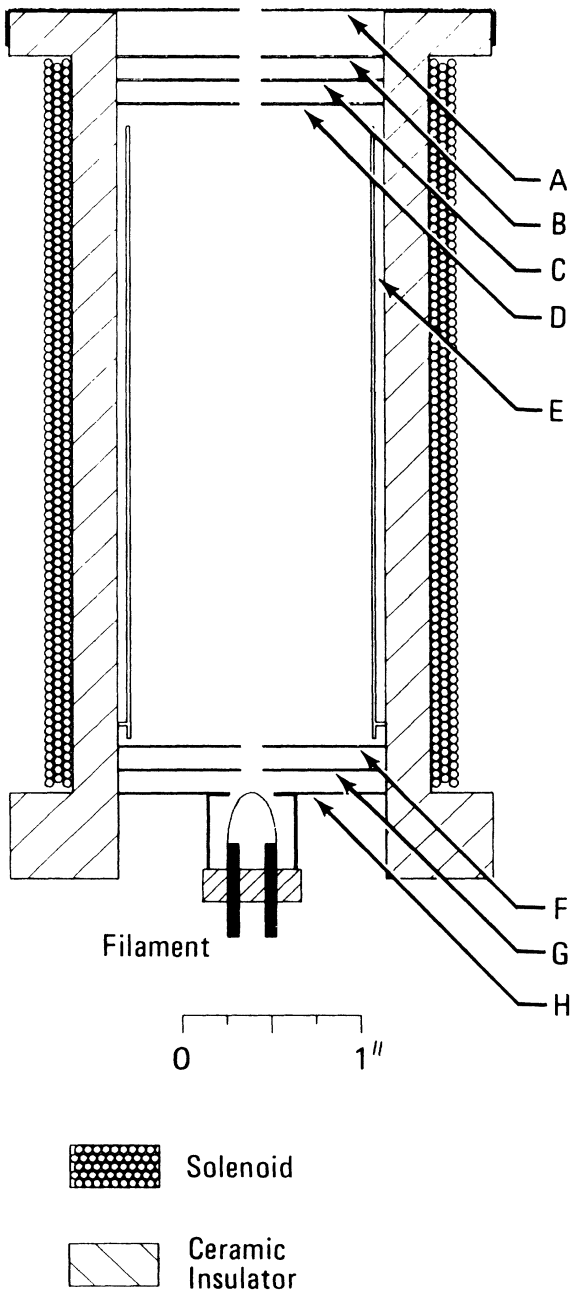

FIG. 2. Low-energy ion gun used in measurements up to 500 eV. Typical electrode potentials with respect to the filament: $V_H=-1.5$, $V_G=117$, $V_F=34$, $V_E=(V_i-V_{fil})=33$, $V_D=31$, $V_C=31$, $V_B=-267$, $V_A=4.8$, for Xe gas.

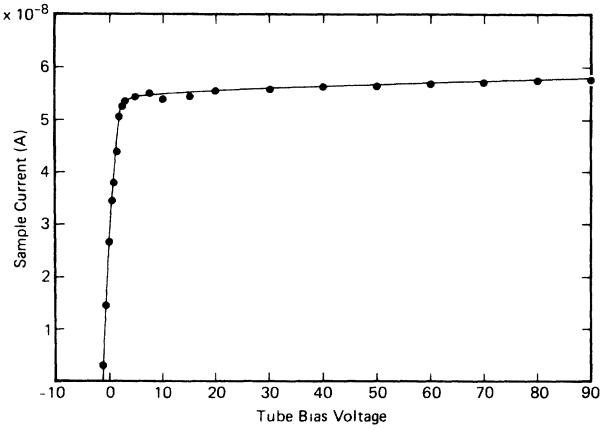

FIG. 3. Current-to-sample vs tube-bias voltage, V_i, between the grounded sample and electrode E.

Measurements with this gun were supplemented by experiments with a commercial ion gun (PHI 20-115), which was employed for most measurements with energies above about 500 eV. For this work the associated electronics were modified so that the focus voltage and the voltages that control the ion and electron energies could be varied continuously. Custom raster electronics were also used in order to produce an ion beam with a square-wave form.

3. *Procedures and calibration experiments*

Measurements are typically made with an ion-beam modulation of 1–3 Hz. The energy input due to the ion beam striking the grounded gold surface produces a modulated heating of the pyroelectric calorimeter, which induces a voltage at the calorimeter's back surface. This modulated voltage is detected using lockin techniques. The output voltage is linearly proportional to the energy input as indicated by the observation that the output signal is linear with ion bombardment current under all conditions. The intercept of the signal versus current curve is close to zero at all ion energies.

The proportionality constant for the calorimeter was established in two independent ways. In the first, the calorimeter surface was illuminated with a ~1-mW He-Ne laser where the optical absorption coefficient was ascertained from reflectivity measurements. This calibration was performed under conditions identical to those of the ion-beam experiments and is estimated to be accurate

to better than 5%. A second method is based on measurement of the amount of energy transferred from a 4000-eV singly charged xenon ion beam to a carbon film for which we assume that the deposition coefficient $f(E_i=4000\text{ eV,Xe})$ is 0.99. This value was demonstrated within experimental error to be independent of energy between about 500 and 4000 eV, and therefore calibrations could be performed over this entire range, although it was typically done at 4000 eV. These two calibrations agree to within their mutual uncertainties. All data reported here have been referenced to scale factors determined by the latter method, i.e., with $f(E_i=4000\text{ eV,Xe})$ taken to be 0.99. We estimate that this value of 0.99 has an uncertainty of the order of a few percent.

This calibration could be routinely employed by depositing carbon onto the gold film and bombarding the detector with a (3000–4000)- eV Xe^+ beam. At first carbon layers were deposited by magnetron sputtering. However, it was soon discovered that carbon (with some hydrogen) that was deposited by bombardment with methane ions produced the same results. Therefore, after measurements for a given substrate material were completed, a carbon layer was deposited using methane ions and the calibration factor determined. A typical value was 15.7 V/W.

Determination of $f(E_i)$ values required measurement of both the total deposited energy and the number of ions hitting the sample. An accurate measurement of the ion current to the sample surface was accomplished by using a Faraday cup with an aperture size identical to that of the calorimeter holder (see Fig. 1). The use of the Faraday cup quite successfully eliminated the influence of secondary electron emission when the PHI ion gun was used. Unfortunately, the magnetic field associated with the ion gun shown in Fig. 2 also focused secondary electrons back out of the Faraday cup. Since the secondary electron yield is relatively independent of energy below about 500 eV, the relative current measurements were accurate, but the absolute values were distorted. This problem did not introduce a large error into the xenon data because the secondary electron coefficient is small. However, the error for helium would have been significant. Therefore, the data for this ion gun was normalized to that of the PHI gun at 300 eV.

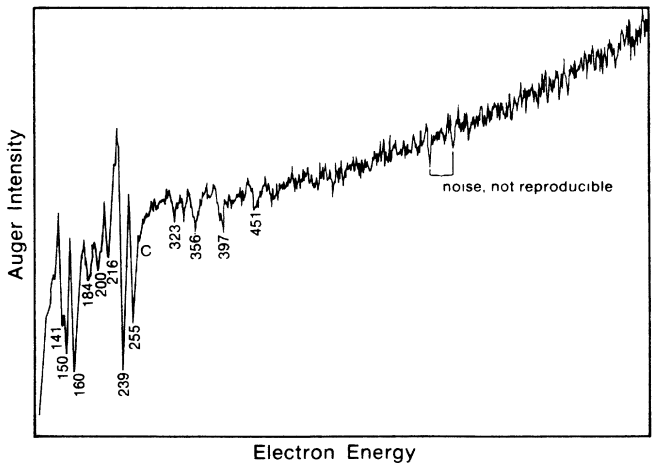

FIG. 4. Auger spectrum for the evaporated gold film deposited on the calorimeter surface. The conditions are believed to be typical of those existing during energy deposition experiments. Gold peaks are designated by their characteristic energy. Carbon is indicated by a C.

It is conceivable that a fraction of a monolayer of a light adsorbate could influence energy transfer to the high-mass-number substrate. It was therefore important to estimate surface contamination levels. The electron beam needed to perform Auger spectroscopy destroyed several calorimeters prior to calibration because of overheating and/or arcing resulting in the loss of data. Therefore, routine Auger analysis was not performed. However, Auger spectra were taken after the data had been accumulated under conditions that were considered to be typical. An example is shown in Fig. 4. The surface is clean except for a small carbon peak, from which we estimate an upper limit for carbon coverage of a few percent of a monolayer.

B. Atomic-beam experiments

In order to determine $f(E_i)$ for even lower values of E_i, and to obtain an independent check of the ion-beam results, we have carried out a separate energy-transfer study over the range 0.1–15 eV using supersonic beams of He, Ar, and Xe atoms incident on a Pt(111) single crystal. A comparison of Pt with Au is justified because the interaction potentials commonly used in collision physics (such as the Moliere, Lenz-Jensen, Thomas-Fermi, etc.) depend only upon the atomic numbers and internuclear separation. Therefore, since Pt is adjacent to Au in the periodic table and has similar chemical and physical properties, we do not anticipate any large quantitative difference in the scattering behavior. The high-energy He, Ar, and Xe atoms are generated in a supersonic atomic-beam source attached to a beam-surface scattering apparatus that has been described in detail previously.[19] Briefly, the supersonic beam is directed at a sample mounted in a UHV chamber on a manipulator that permits accurate control of the surface temperature and incidence angle. The beam energy is varied by changing the nozzle temperature (up to 2200 K) and can be determined from atom flight times between a high-speed chopper and a differentially pumped rotatable mass spectrometer.[19] The chopper is situated at a distance of 10.7 cm from the sample and rotates at 400 Hz to give beam pulses of about 7 μs full width at half maximum (FWHM). The rotatable mass spectrometer is a further 10 cm from the sample. Time-of-arrival distributions at this detector are analyzed to obtain the energies of scattered species, as described elsewhere.[19] We also measure angular distributions of scattered atoms by rotating the mass spectrometer around the sample and recording the signal versus angle using phase-sensitive detection referenced to the chopper.

III. RESULTS

A. Ion-beam results

Figure 5 shows the energy deposited per incident ion into a gold lattice as a function of the incident kinetic energy, E_i of the impinging ions in the range 5–100 eV. It is apparent that the energy deposition increases more or less linearly with E_i over this range. It is also apparent that significant energy is deposited in the limit of zero kinetic energy. This suggests a relationship for the deposited energy, E_d, of the form:

$$E_d = E_d^{\mathrm{KE}}(E_i) + E_d^0 , \tag{1}$$

where $E_d^{\mathrm{KE}}(E_i)$ is a component of the deposited energy that depends on E_i, and E_d^0 represents an energy deposition that is independent of kinetic energy and is given by the zero-energy intercept of the E_d versus E_i curve. We will argue in the following that the energy-dependent term, $E_d^{\mathrm{KE}}(E_i)$ must be very close to $f(E_i)E_i$, where $f(E_i)$ is the fraction of the ion kinetic energy deposited in the lattice.

In addition to the transfer of ion kinetic energy to the surface, there are at least two other processes intrinsic to the ion-surface collision process that effect the overall energy increase of the sample and its temperature rise, which is ultimately the quantity measured by the pyroelectric detector. The first of these is energy loss due to secondary electron emission, which reduces the net energy deposited by an amount E_e. This loss is likely to be negligible for Xe^+, but could be as much as 5 eV per ion in the case of He^+.[20] In all cases we expect only a weak dependence of this loss on E_i, so that E_e will contribute predominantly to E_d^0. A second potentially important process is damage to the lattice due to atomic displacements resulting from ion bombardment. This disordering could certainly store energy relative to the defect-free substrate. However, all results reported here refer to an approximately steady-state condition of the sample after fairly long-term bombardment. We presume therefore that there are roughly a constant number of such displacements and that it is unlikely that such effects will significantly affect E_d, particularly in the low-energy range where they would be most significant to our analysis.

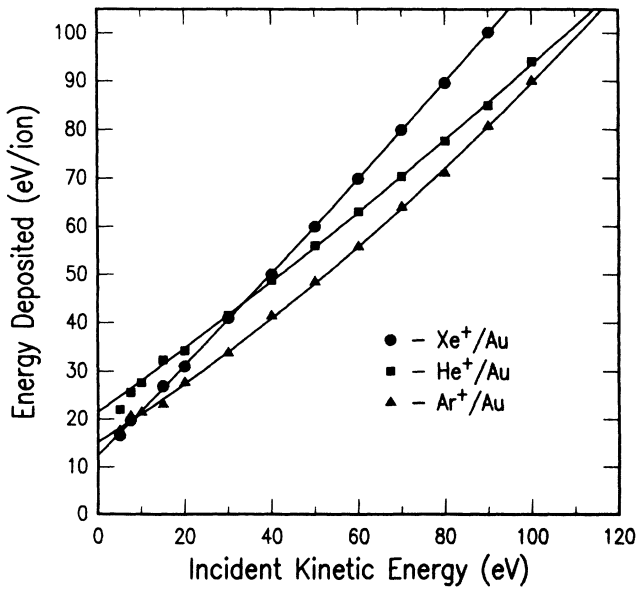

FIG. 5. Energy per ion deposited into the gold surface of a pyroelectric calorimeter as a function of incident kinetic energy for Xe^+, Ar^+, and He^+, for an incidence angle of 0°.

In addition to these effects, which would *reduce* the deposited energy measured calorimetrically, extra energy may be deposited inadvertently by incident neutrals, x rays and electrons emanating from the ion gun. However, we believe that the net effect of these terms must be either small or relatively independent of E_i. Thus we calculate $f(E_i)$ assuming

$$E_d = f(E_i)E_i + E_d^0 , \tag{2}$$

where E_d^0 is found by extrapolating the data in Fig. 5 to $E_i = 0$, identifying it with the low-energy intercept as already mentioned. We then take

$$f(E_i) = \frac{E_d - E_d^0}{E_i} . \tag{3}$$

Support for this approach comes from the fact that for Xe^+ at $E_i = 100$ eV, where we expect $f(E_i) \sim 1$, and $f(E_i)E_i \simeq 100$ eV, we find $E_d = E_d^0 + 100$ eV, to within the accuracy of the measurements (±2 eV). That is to say that the total energy deposited exceeds that due to the estimated transfer of ion kinetic energy by an amount very close to E_d^0.

The actual E_d^0 values obtained are 12±1 eV for Xe, 15±2 eV for Ar, and 22±3 eV for He. These values are remarkably close to the ionization potentials (IP's) of the gas phase atoms, which are 12.1, 15.8, and 24.6 eV, respectively. There is no obvious reason why these two sets of numbers should be so close, since the neutralization energy for the ions is expected to be IP minus ϕ, where ϕ ($\sim$5.3 eV) is the surface work function for gold. Although the thermodynamics of the calorimeter–electronic circuit system are subtle, we do not believe that it would be physically correct to identify E_d^0 with the IP values, because to gain the full IP on neutralization would require a source of electrons at vacuum potential that can be "donated" to the calorimeter, to liberate an energy equal to ϕ, thereby canceling the work function term. However, considering the experiment as a whole, one can argue that the electron that is originally removed from the atoms in the ion gun is likely to deposit "work function energy" into the ion gun. This being so, any scheme where these ions are later neutralized without providing work function energy could be potentially used to violate energy conservation.

We conclude that the measured intercepts are roughly 5 eV higher than the ion neutralization term. One possible explanation of this, that there is an offset in the energy calibration of the ions, seems to be ruled out by careful

measurements of retarding potential curves such as that shown in Fig. 3. Such measurements always indicate that the ion kinetic energy is very nearly equal to the tube bias voltage with respect to the (grounded) sample, V_i. If this calibration is correct, then either the ion current value used is too low or additional net energy per ion is actually being deposited by some process such as those already mentioned. Since the Faraday cup current measurement is believed to be accurate, we suspect that an additional mechanism for energy transfer is operating. For example, it is possible that energy could be deposited by electron bombardment of ion-induced secondary electrons from electrode B, which could be partially focused into the calorimeter by the line-space charge associated with the ion beam, and could arrive at the sample with two or three hundred eV of energy. Only one or two high-energy electrons per 100 incident ions would carry sufficient energy to account for the additional energy deposition measured here.

Figure 6 displays the values of $f(E_i)$ calculated using Eq. (3) and the data in Fig. 5 for He^+, Ar^+, and Xe^+ ions incident on the gold surface with E_i in the range 5–500 eV. Curves showing $f(E_i)$ with E_i ranging up to 4000 eV are displayed in Fig. 7. The data show that over 95% of the incident kinetic energy is deposited into the lattice by Xe ions with energies above 10 eV. For Ar and He the fraction of kinetic energy deposited is less, but is always greater than 60% for $E_i \geq 5$ eV. The reproducibility of these values for different calorimeters and for runs taken over a long period of time is about 3% for Ar^+ and

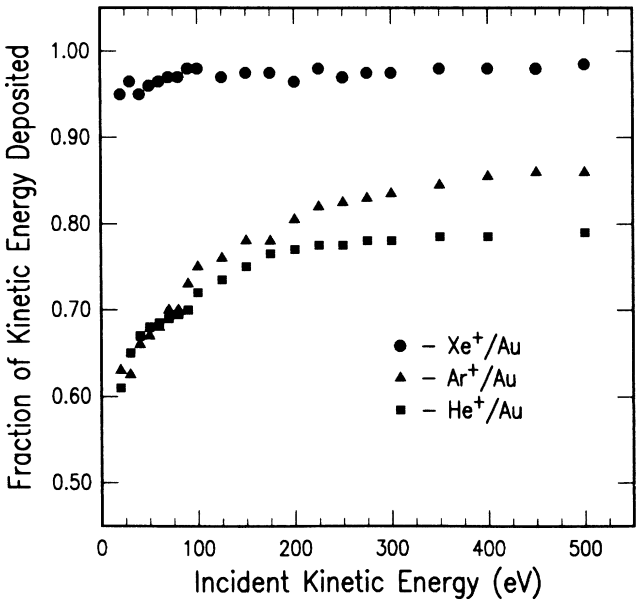

FIG. 6. Fraction of the kinetic energy of Xe^+, Ar^+, and He^+ deposited in gold for an incidence angle of 0° and incidence energies up to 500 eV. These results were obtained from the data in Fig. 5 by subtracting the energy deposited in the limit of low kinetic energy, i.e., the zero-energy intercept. See the text.

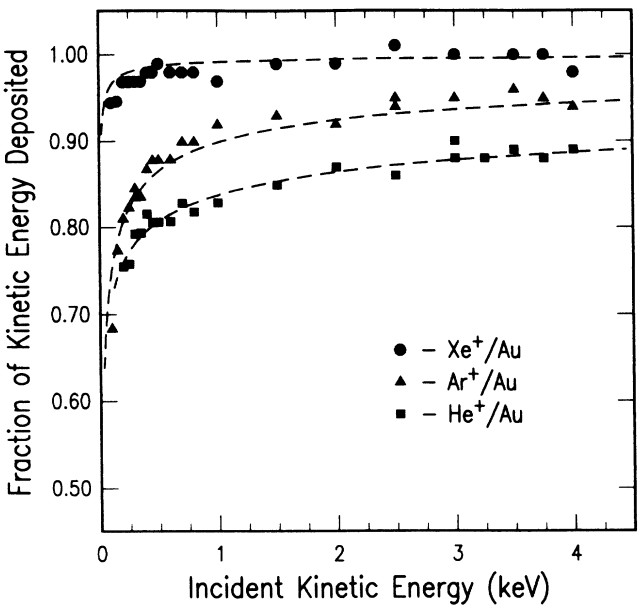

FIG. 7. Fraction of the kinetic energy of Xe^+, Ar^+, and He^+ deposited in gold for an incidence angle of 0° and incidence energies up to 4000 eV.

Xe^+, and about 4% for He^+. The short-term reproducibility is much better. The difference between long-term and short-term reproducibility suggests that surface morphology, surface structure, and the presence of embedded, noble-gas atoms may slightly change the measured values for deposited energy. These are small effects, however, which are not important to any of the conclusions drawn in Sec. IV.

It is expected that the amount of energy deposited into the surface will depend somewhat on the degree of roughness,[21] which for example, will effect the mean number of collisions with the surface prior to reflection. Roughness is a parameter that is difficult to measure or control. The calorimeter itself has some inherent roughness as indicated by a typical scanning electron microscopy (SEM) photograph shown in Fig. 8(a). The deposition of evaporated films may produce additional roughness, and ion bombardment can also cause the roughness to change. This can be qualitatively seen from the SEM photographs of lightly and heavily ion bombarded gold surfaces shown in Figs. 8(b) and 8(c), respectively. As a check for effects of roughness, energy deposition was measured for three different calorimeters that had gold surfaces that had been exposed to different ion fluences. We find that the fraction of kinetic energy deposited is within ±2% of the mean for the three calorimeters across the full range measured. As indicated by the micrographs in Fig. 8, the apparent roughness of the samples at that magnification (10 000×) is very different; nevertheless, the amount of energy deposited is quite similar. It is possible that differences in roughness on a finer scale still might be important for kinetic-energy deposition, but unfortunately, we were unable to get good micrographs with higher magnification for these samples, so we cannot evaluate

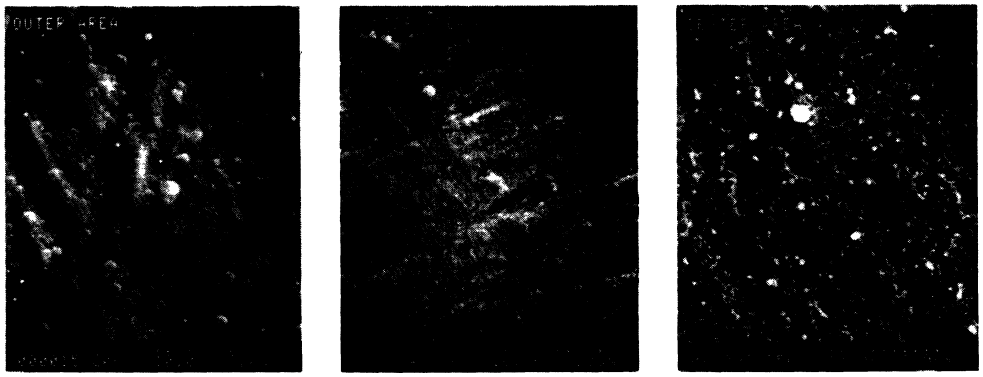

FIG. 8. Scanning electron micrograph of the gold surface. (a) Unbombarded area. (b) Lightly bombarded sample. (c) Heavily bombarded sample used in most of these experiments. The white dots indicate a length of 3 μm.

this possibility.

Figures 9(a)–9(d) show x-ray patterns for a gold powder standard and for evaporated gold films that were subjected to varying doses of ion bombardment. The as-deposited gold films were preferentially oriented in the [111] directions as can be seen by comparing Figs. 9(a) and 9(b). Comparison of the x-ray spectra for the unbombarded surface [Fig. 9(b)] with that of the lightly bombarded surface [Fig. 9(c), corresponding to Fig. 8(c)] indicates that the orientation changes somewhat with ion dose. A marked difference is observed between the lightly bombarded sample [Fig. 9(c)] and the heavily bombarded sample [Figs. 9(d) and 8(c)]. Despite this evidence for considerable crystallographic changes, as already noted, these changes did not cause a large change in the fraction of ion kinetic energy deposited.

B. Atomic-beam results

While ion-beam measurements are well suited to studies above 10 eV or so, they are not suitable for estimating $f(E_i)$ or $R(E_i)$ for lower energies because at such low energies uncertainties in the ion energy distribution and E_d^0 become increasingly important. We have therefore supplemented the ion-beam measurements with atomic-beam studies that can be extended to arbitrarily low energies. In this case we employ hydrodynamic accelerations using conventional supersonic molecular-beam techniques.[22] By heating our nozzle to 2200 K and seeding in H_2, we have obtained Xe and Ar beam energies as high as 14.3 and 7.2 eV, respectively. For these two atoms measurements were not made below about 1 eV, since the results would be sensitive to the attractive well ($\sim$0.3 and 0.1 eV for Xe and Ar, respectively) and to the surface temperature in this thermal scattering regime. Thus trapping becomes important for Xe below about 0.5 eV and Ar scattering can be superelastic, with $f(E_i)<0$ at low energies,[23] where surface thermal energy may be transferred to translational motion of the scattered atoms. In the case of He, such effects are less important, since the well depth is very small (<0.01 eV) and the atoms move at high velocities for a given energy, making energy transfer from the surface inefficient. On the other hand, we were unable to obtain He energies above 0.6 eV because only H_2 is available as a lighter carrier gas, and the mass ratio gain in energy given by seeding is limited to a factor of 2.

Rather than using a direct calorimetric technique, energy deposition was estimated in this case from detailed measurements in which we obtained velocity and flux distributions for scattered atoms as a function of scattering angle. This process is illustrated in Fig. 10, which shows a plot of the kinetic energies of Xe atoms after scattering from an 800-K Pt(111) surface at angles between 5 and 65° from the surface normal. Here the incident atoms had an energy of 6.8 eV (with a FWHM spread of <1 eV) and collided with the surface at an angle of 30° from the normal. Also shown in this figure is the angular distribution for the scattered species. Averaging the energies over this angular distribution gives a value for the mean energy of the scattered atoms of $\langle E_f \rangle = 2.3$ eV, which is marked as a dashed line in the figure. In this case we obtain

$$f(E_i = 6.8 \text{ eV}) = 1 - 2.3/6.8 = 0.66 .$$

Note that this result strictly applies only to those atoms scattered in the plane defined by the beam axis and the surface normal. However, careful comparison of the observed flux distribution in this plane with the measured total beam intensity indicates that the scattering distribution has a similar width out of plane, suggesting that similar inelastic energy losses would be observed for atoms scattered out of plane.

Results such as those displayed in Fig. 10 have been obtained for incidence angles of 15°, 20°, 30°, 45°, and 60°. Extrapolation to $\theta_i = 0°$ then provides estimates for $f(E_i)$ at normal incidence, for comparison with the ion-beam work. Measurements could not be made at $\theta_i = 0°$ directly, as this involved aligning the beam along the surface

normal, in which case angular scans of the detector would be restricted to large scattering angles by the machine geometry. Figure 11 is a summary plot showing the variation of the fraction of kinetic energy deposited by He, Ar, and Xe atoms colliding with the Pt(111) surface versus incident energy. For each atom the data covers the accessible energy range. These results were obtained at a surface temperature of 800 K, but $f(E_i)$ is found to be relatively insensitive to this temperature for energies above 1 eV. It is seen that the inelasticity is

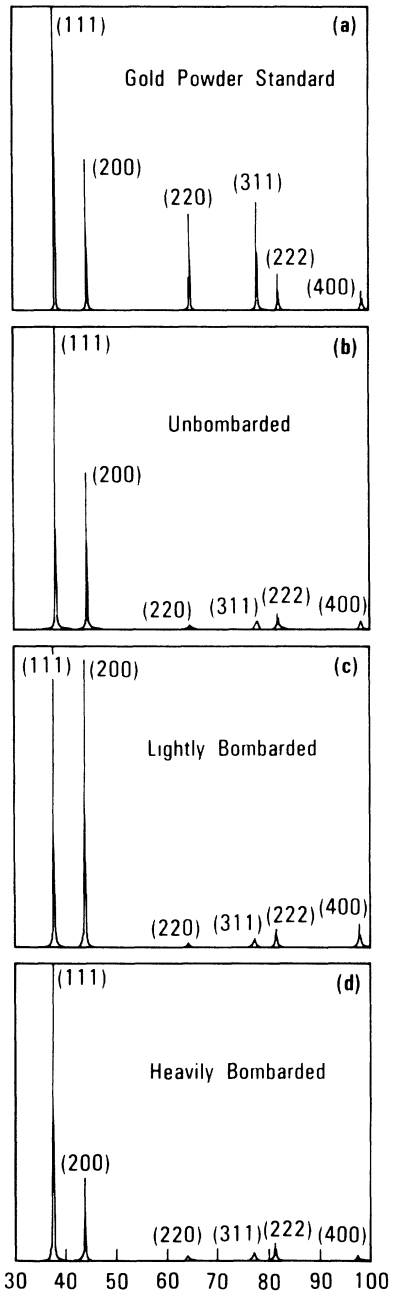

FIG. 9. X-ray spectra of various samples. (a) Gold-powder standard. (b) Unbombarded area of gold film. (c) Lightly bombarded area. (d) Heavily bombarded calorimeter on which the low-energy data was taken.

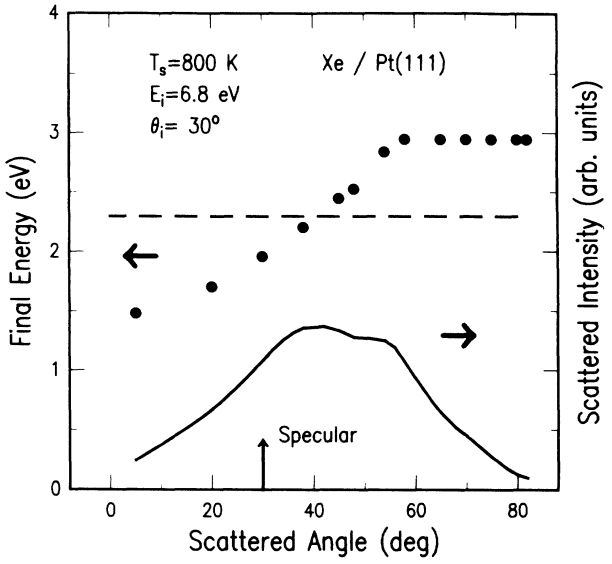

FIG. 10. Mean final translational energies of Xe atoms scattered from Pt(111) at different final angles. Here the incidence energy was 6.8 eV, the incidence angle 30° with respect to the surface normal, and the surface temperature 800 K. The dashed line indicates the overall mean over all final angles obtained by appropriate averaging over the angular distribution that is displayed as a solid curve.

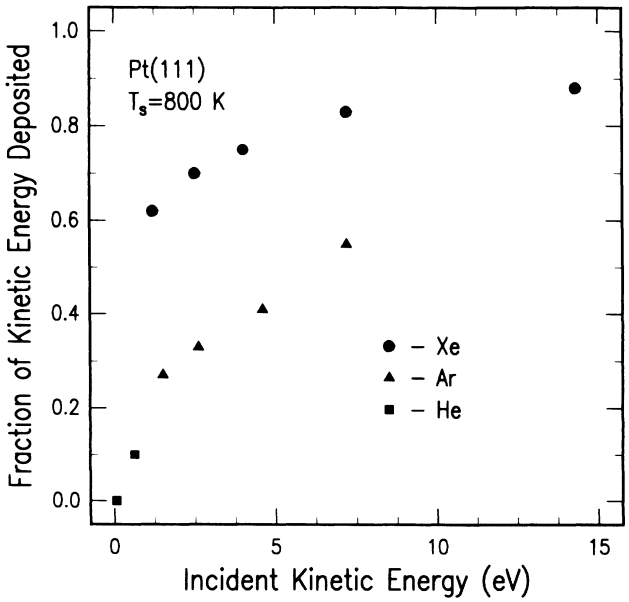

FIG. 11. Fraction of the kinetic energy of Xe, Ar, and He atoms deposited into Pt(111) for normal incidence and a surface temperature of 800 K.

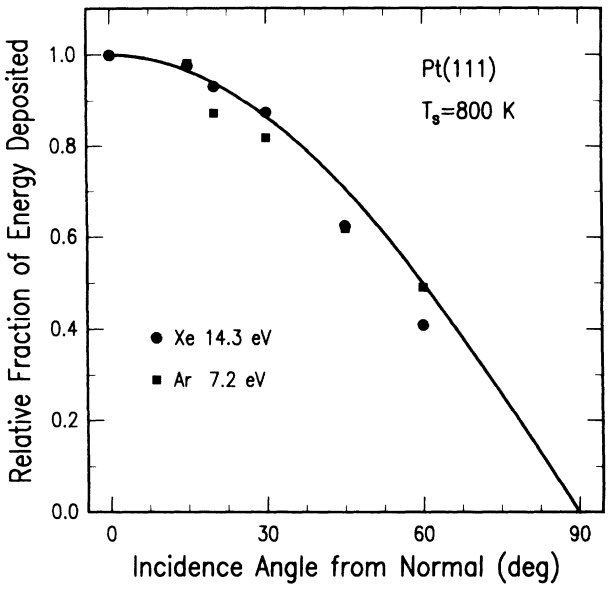

FIG. 12. Relative fraction of the kinetic energy of 14.3 eV Xe and 7.2 eV Ar atoms deposited into Pt(111) as a function of incidence angle normalized to that for normal incidence. The solid curve shows a cos θ_i dependence. The surface temperature was again 800 K.

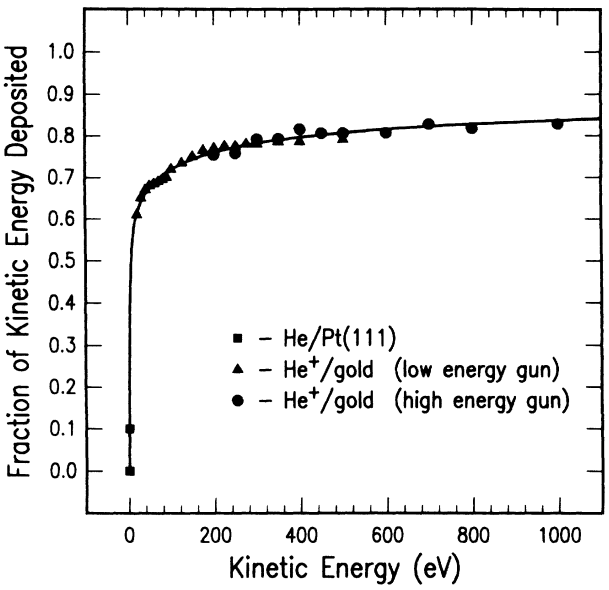

FIG. 13. Composite curve displaying the fraction of the kinetic energy of He^+ and He deposited into Au and Pt(111) surfaces. Note that the ion data were obtained with two different ion guns, as labeled. The curve represents a nonlinear least-squares fit to the data based on Eq. (4), as discussed in the text.

greatest for Xe at high energies, with $f(E_i) > 90\%$, while for He at low energies the scattering is almost perfectly elastic.

As already mentioned, energy deposition is expected to be affected by surface roughness. The results obtained for different incident angles permit us to quantitatively assess this effect. Figure 12 shows how energy deposition varies with incidence angle for the highest-energy Xe and Ar beams. Specifically, a plot is given of the relative fraction of kinetic energy transferred to Pt(111) as a function of incidence angle, normalized to the value measured at $\theta_i = 0$. Interestingly, we find that the deposited energy decreases roughly as $\cos\theta_i$, i.e.,

$$f(\theta_i)/f(\theta_i = 0°) \sim \cos\theta_i \ .$$

Such a dependence is indicated by the solid line in Fig. 12. This simple empirical relationship can be used to estimate the energy deposited into an arbitrarily rough surface. It can be demonstrated that if the spatial frequency spectrum is "white" (a rather severe assumption) down to a minimum length scale described by a wavelength λ, the mean value of $\cos\theta_i$, for particles incident along the mean surface normal is given by $(1-\pi^2\delta z^2/\lambda^2)$, where δz^2 is the mean-square height variation of the surface, and it is assumed that $\delta z \ll \lambda$.

C. Comparison of ion- and atomic-beam results

It is natural at this point to try to relate the measurements of energy deposition for ions and atoms so that we may give a unified description covering the entire range of energies examined. Indeed there is an intrinsically close relationship between the two types of processes involving ions and atoms colliding with a metal surface, since at low energies the ion is expected to be neutralized by an electron from the metal before it actually encounters the hard wall repulsive potential. There are two major differences between the ion-beam and atomic-beam

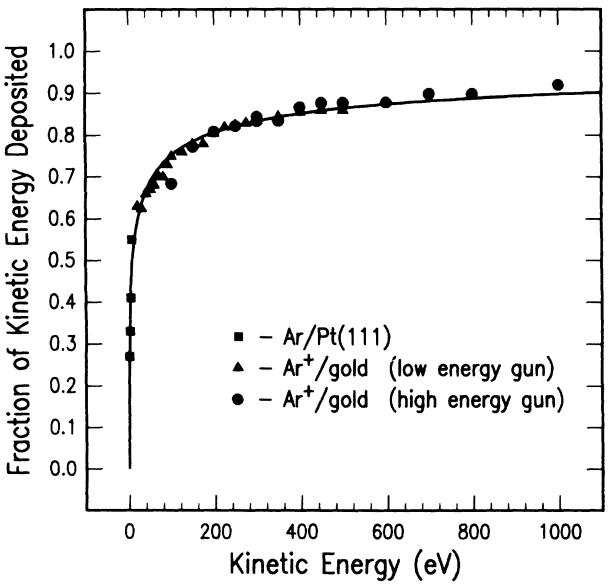

FIG. 14. Composite curve displaying the fraction of the kinetic energy of Ar^+ and Ar deposited into Au and Pt(111) surfaces. The curve represents a nonlinear least-squares fit to the data based on Eq. (4), as discussed in the text.

studies. First, comparing energy transfer from ions with that from atoms requires care. In particular, the image potential seen by an ion as it approaches a metal surface will accelerate it somewhat, thereby converting electronic to kinetic energy.[24] It can be estimated that an ion could gain up to 3 eV in this process, prior to the "hard" collision with the surface. At the same time, the amount of electronic recombination energy gained when the ion is finally neutralized also varies with distance from the surface in such a way that as the ion kinetic energy increases, the recombination energy decreases by an equal amount. Thus the "kinetic" energy scales in Figs. 6 and 7 have a slight ambiguity with respect to the atomic-beam case. Second, it is not intuitively obvious that energy transfer to a polycrystalline Au surface should necessarily be the same as to a Pt(111) surface. The samples differ both in the nature of the metals and their morphology. We do not, however, believe that there should be major differences between Pt and Au as far as these measurements are concerned since, as was mentioned earlier, the interaction potentials and masses are similar. We expect the atomic mass to be the most important energy-transfer parameter in the structure scattering regime, and these two elements differ in mass by only 1 amu. Morphologically, these two surfaces are again quite similar, with the Au preferring to expose ⟨111⟩ facets and having a lattice spacing only 4% bigger than for Pt. However, we note that the Debye temperature and melting point of Pt are 35% and 66% higher than Au, respectively, suggesting that Pt is appreciably harder. This could conceivably influence energy transfer at the very lowest energies.

The preceding reservations aside, it is clear from Figs. 6 and 11 that the ion- and atomic-beam studies are basically in good agreement, and thus we are encouraged to construct composite curves from these two sets of data. The combined results showing the fraction of kinetic energy transferred to the metal by Xe, Ar, and He, respectively, are displayed in Figs. 13–15. The gradual decrease in energy-transfer efficiency with falling incident energy accelerates sharply at very low E_i. Also shown in these figures are fits to the Ar and Xe data based on the empirical function:

$$f_1(E_i)=[1+(E_i/a)^{-b}]^{-1} . \tag{4a}$$

For the He data we found that a much better fit was obtained if the function in Eq. (4a) was multiplied by an additional term:

$$f_2(E_i)=[1-\exp(-E_i/c)]f_1(E_i) . \tag{4b}$$

Optimum nonlinear least-squares fits were obtained over the full range of the data up to 4000 eV. Best fits were obtained for He with $a=4.44$ eV, $b=0.303$, and $c=1.923$ eV; for Ar with $a=9.73$ eV and $b=0.472$; and for Xe with $a=0.577$ eV and $b=0.644$. These functional forms were chosen rather arbitrarily because they give quite accurate representations of the measured data. They do not have an obvious physical basis, and thus we caution the reader against extrapolation beyond the range of the measurements. For completeness, Fig. 16 displays semilog plots of the fitted curves for the three species.

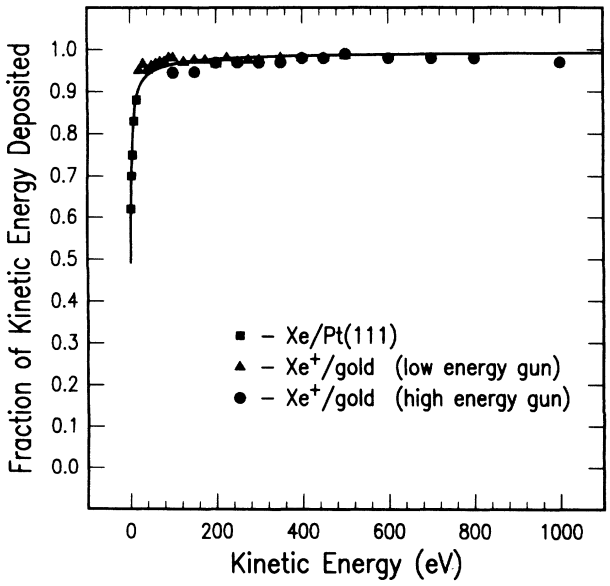

FIG. 15. Composite curve displaying the fraction of the kinetic energy of Xe^+ and Xe deposited into Au and Pt(111) surfaces. The curve represents a nonlinear least-squares fit to the data based on Eq. (4), as discussed in the text.

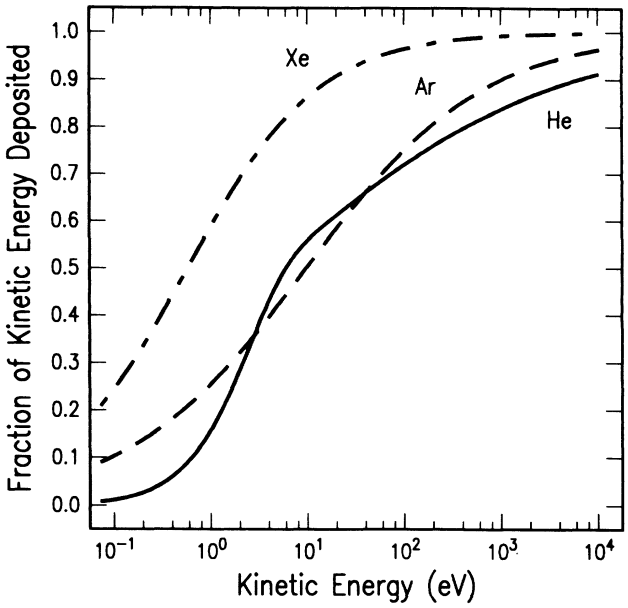

FIG. 16. Summary of results for the fraction of kinetic energy loss to Au (Pt) by He, Ar, and Xe. These curves are the fitted curves displayed in Figs. 13–15 and based on Eq. (4).

IV. DISCUSSION

A. High-energy collision dynamics

Most modern approaches to the theory of ion-solid collisions at high (keV) energies are based on the binary-

collision model, which assumes that incident particles lose energy and momentum to a solid by way of a series of binary or isolated collisions. Physical sputtering, for example, can be modeled as a multiple-collision process involving a cascade of moving atoms. The essence of this model is that energy transfer essentially occurs to one collision partner at a time. That is to say any given trajectory can be thought of in terms of a series of encounters in which the incident atom or ion sequentially strikes single target atoms. However, such a picture is not expected to be valid for arbitrarily low energies. For example, Robinson and Torrens[25] have discussed the limitations of the binary-collision model and suggested that it is inappropriate for copper atoms moving through a copper lattice below about 9 eV, and below 33 eV for gold atoms moving through a gold lattice.

The incident species can interact with and simultaneously accelerate more than one substrate atom in one of two ways, leading in either case to a breakdown of the binary-collision approximation. One possibility is that for sufficiently low energies the distance of closest approach to the surface is comparable to or greater than the lattice spacing, so that the effective interaction must involve several substrate atoms. Carter[26] has summarized the work of Arifov[27] and Gurvich[28] who showed that this situation could be modeled by assuming that the struck atom had a large "effective mass." A second possibility is that even when the collision range is relatively short, several lattice atoms may be accelerated at once via bonds between the "struck" atom and other substrate atoms. For example, if the substrate bonds were infinitely stiff, the incident atom would need to transfer momentum to the whole crystal at once, and the effective mass of the target would be that of the crystal. A crude estimate of the energies below which this kind of "collective" response could be expected can be derived by equating the velocity of the incident particle to the sound velocity of the metal (about 3250 m/s for both Pt and Au). This gives an energy of 55 meV/amu, or 0.22, 2.2, and 7 eV for He, Ar, and Xe, respectively. Both of these effects can be expected to be negligible at sufficiently high energies, where turning points are small compared to the distances between atoms and when the target atom moves a negligible distance during the time of an encounter.

Since energy transfer from Ar^+ to gold, for example, is more efficient than to a particle several times as heavy as gold, we expect that an increased effective mass at low ion energies would lead to an increase in reflected ion kinetic energy compared to the predictions of a binary-collision model. This increase of reflected energy is not observed for incident ion energies down to at least 20 eV. Considering the uncertainties in both the experiment and calculations, we conclude that the data in Figs. 5–7 are consistent with the TRIM code calculations of Eckstein and Biersack,[29] which are based on the binary-collision approximation. However, it is possible that an increase in effective mass is responsible for the sharp decrease in energy deposition at the very lowest energies (see Figs. 13–15). In particular, the rapid rise in reflected energy observed in the atomic-beam studies over the 1–10 eV range could be interpreted in terms of a corresponding increase in effective mass over this range. To test this idea, we consider the energy-transfer dynamics in terms of a hard cube model,[30] which is found to successfully account for a wide range of results in the low-energy regime.[31,32] Here the scattering process is modeled in terms of an equivalent collision between the incident atoms and a single cubic target atom of a given mass. Neglecting any attractive interaction, we find for Xe and Ar colliding with Pt(111) at 10 and 7 eV, respectively, that our results are consistent with an effective mass of ~ 1.5 Pt atoms in both cases, rising to about 5 Pt atoms in both cases below about 1 eV. We believe that this behavior mostly reflects the fact that with increasing energy the turning point moves in toward the surface, leading to stronger interactions with fewer atoms. Rough estimates for the turning point of Ar approaching Au, on a potential of the Lenz-Jensen type,[33] support this conclusion, since for this case the turning point varies from ~ 2.5 Å at 1 eV, to 1.7 Å at 10 eV, compared to the lattice spacing of 2.9 Å. Angular distribution measurements are also consistent with this picture. For example, the width of such distributions pass through a minimum in the region of 1 or 2 eV, becoming broader again at higher energies.[34–38] The high-energy broadening is attributed to so-called "structure scattering,"[34] which occurs when the incoming atom senses the structure of the individual surface atoms.

Once the distance of closest approach is short compared to the lattice spacing, incident atoms will on average only be reflected after two or more sequential collisions, leading to higher-energy losses. To detect deviations from the predictions of an isolated binary-collision model in this case requires more detailed simulations, such as those based on the so-called "TRIM code."[29] From the simulations of Eckstein and Biersack[29] we estimate $R(E_i)$ values for He, Ar, and Xe colliding with Au at 1000 eV of 0.25, 0.10, and 0.01, respectively, which is in reasonable agreement with our data. Thus our estimates can only provide limited insight into the dynamics of what may ultimately be a rather complex scattering process. Nevertheless, our results are not inconsistent with the assumption that an isolated binary-collision model may be a reasonable approximation for energies above about 20 eV or so.

B. Lattice penetration

Increasing the energy of incident atoms or ions beyond the point where the distance of closest approach falls appreciably below half the lattice spacing will on average cause them to penetrate deeper and deeper into the lattice before being reflected back into the vacuum. Eventually some may become trapped or implanted. Since this requires lattice disruption, one expects the threshold energy for trapping to exceed the bulk displacement energy. Thus implantation may be energetically possible at 10 or 20 eV. However, it may remain an improbable process up to much higher energies. An indication of lattice penetration would be the observation of energy deposition levels requiring large numbers of binary collisions. Although trajectory calculations would be needed to

make a definitive statement, it seems very unlikely that an incident ion would make more than three or four collisions unless it penetrated at least the first atomic layer of the lattice. The maximum energy that can be transferred in a collision between two atoms is given by

$$T_{\max}=\frac{4M_1M_2}{(M_1+M_2)^2}E_i=\gamma E_i \ , \tag{5}$$

where M_1 and M_2 are the masses and E_i is the incident energy. We then obtain $\gamma=0.96$, 0.56, and 0.08 for Xe, Ar, and He on gold. The *average* energy loss will be considerably lower. Using the low-energy cross section suggested by Sigmund,[39] the average energy transfer is estimated to be less than one half (possibly one third) of these values. Therefore, for 20 eV Ar and Xe to lose 60% and 95% of their energy, as indicated by Fig. 6, on average should require up to five such collisions, while for He to lose 60% of its energy requires more than 25 collisions. This latter number for He is so large that we believe that lattice penetration must be occurring in this case even at 10 eV. The Ar and Xe energy losses could in principle be achieved in one or two collisions if these were to involve close-to-optimum energy transfer. Such a high probability for strong collisions could arise if the surface potential were to "steer" the incoming atoms towards low-impact parameter collisions. However, in the absence of such "steering," the large average number of collisions strongly suggests that Ar penetration is occurring at energies as low as 50 eV, where the energy transfer of 75% approaches that expected for even two strong collisions. Indeed, even the ~50% energy loss for Ar close to 10 eV could in principle be due to a fraction of the incident species penetrating. At lower energies, however, in the range of the atomic-beam experiments, the quasispecular angular distributions observed, together with the associated velocity distributions argue against appreciable penetration. The increased energy transfer in this low-energy range is instead attributed to effective-mass effects, as already discussed.

It is also possible to view the large fractional energy-transfer results [$f(E_i)>60\%$, for He and Ar and $>95\%$ for Xe], in terms of nuclear-stopping-power formalism of Lindhard and Sigmund,[39,40] using an interaction potential appropriate for the relatively low particle energies of interest here. In this treatment, the rate at which an energetic ion (neutral) loses energy as it travels through a lattice is given by[41]

$$\frac{dE}{dL}=-nS_n(E)\equiv-n\int_0^{T_{\max}}Td\sigma \ , \tag{6}$$

where n is the atom density, $S_n(E)$ is the nuclear stopping power for density n and a particle energy E, T is the energy transferred in a collision, $d\sigma$ is the differential cross section for transfer of energy between T and $T+dT$, $T_{\max}$ is the maximum possible energy transfer, and L is the distance traveled through the lattice. Following Sigmund, and using an inverse power potential approximation to a Born-Mayer potential (i.e., $m=0$), the stopping power at low energies becomes

$$S_n(E)=C_0\left[\frac{4M_1M_2}{(M_1+M_2)^2}\right]E \ , \tag{7}$$

where C_0 has traditionaly been taken to be 1.81 Å (but its value is somewhat uncertain and may be as much as twice that large). Substitution of (7) into (6), followed by integration and algebra, leads to

$$L=\frac{-1}{nC_0\left[\frac{4M_1M_2}{(M_1+M_2)^2}\right]}\ln\left[\frac{E}{E_i}\right] \ , \tag{8}$$

where E_i is the incident energy, and E is the remaining energy of the ion after it has traveled a distance L. We infer from our data that at 20 eV an average incident particle would leave the surface with a fraction $E/E_i=0.4$ (He,Ar) and $E/E_i=0.05$ (Xe) of its incident energy. The corresponding distances from Eq. (8) that these particles would need to have traveled through the lattice to suffer the observed energy losses are 107 Å for He, 31 Å for Ar, and 15 Å for Xe. These distances are not precisely defined, since atoms traveling along a surface might require longer paths to lose a given amount of energy, while an increased value of C_0 or perhaps some "focusing" or "steering" effects could increase the effective stopping powers and reduce the travel distances required to obtain the observed energy losses. Despite these uncertainties, it seems clear that for a 20 eV He ion to lose half of its incidence energy it must penetrate the lattice and suffer numerous collisions prior to being trapped or reflected back into the gas phase. For Ar and Xe the situation at this energy is much less clear cut, since the estimated travel paths are of the order 2–10 lattice spacings long. However, if these range estimates are even approximately correct, they would suggest that at 20 eV some of these particles may first penetrate the first atomic layer before returning to the gas phase.

C. Trapping probabilities

Kornelsen[42] has measured the probability that noble-gas ions of a given energy will be trapped in the lattice. For Ar on tungsten (mass 183.85) the trapping probability is very small (<0.1) for ion energies below 100 eV. Close and Yarwood[43] suggested that it was reasonable to assume that the ion would be trapped if it penetrated the lattice, and reflected if it did not. If this were the case then Kornelsen's data could be interpreted as an indication that lattice penetration decreases rapidly for ion energies below 100 eV. An alternative interpretation is that permanent trapping requires that the incident argon becomes embedded several atomic layers beneath the surface. Atoms that fail to penetrate to such depths diffuse back to the surface and are desorbed into the gas phase. We believe that these results favor the latter interpretation since, as we already argued, penetration of the first atomic layer is probably occurring for E_i as low as 50 eV for Ar. Moreover, Fig. 14 shows that the energy transferred by Ar increases gradually over the range 20–100 eV to a point where the overall energy transfer appears to be beyond what could reasonably be expected

in the absence of penetration. It seems likely then that the first surface layer is penetrated at relatively low energies, but at these energies the atoms are rarely trapped. This would imply that the hypothesis of Close and Yarwood is incorrect and that Kornelsen's data yields little definitive information about lattice penetration.

D. Physical sputtering

Sigmund's theory[39] of physical sputtering suggests that the yield (atoms per ion) is proportional to the quantity of energy deposited in a narrow region close to the surface. Moreover, at low energies most of the transferred energy is expected to be deposited within a few Å of the surface. For example, less than 1% of 500 eV Xe^+ ions penetrate more than 7.5 Å into tungsten,[44] and similar results would be expected for gold. Therefore, if the theory were applicable, it might be expected that the sputter yield would simply be proportional to the total deposited energy. Unfortunately, experimental data is generally presented as a function of incident ion energy rather than of deposited energy. One of the original motivations of this research was to provide the data necessary to convert from incident to deposited energy in order to determine whether the use of this parameter would make comparison with theory more meaningful and lead to additional insight. Following this idea, Wehner's[45] sputter-yield data was plotted as a function of deposited energy in the range up to 500 eV. Results for Ar^+ (Fig. 17) clearly exhibit a nonlinear behavior. Similarly, since Fig. 6 shows that the deposited energy and incident energy are almost equal for Xe^+ on gold, one can simply examine Wehner's original data and see that it is also nonlinear. These experiments, therefore, suggest that in this low-energy regime the sputter yield is not in fact strictly proportional to energy deposited into the surface region. This result is not particularly surprising since Sigmund always believed that the theory would be somewhat inaccurate at low energies.

It is also interesting to estimate the fraction of energy carried away by sputtered-gold atoms. The reflected kinetic energy at 100-eV incident energy is about 28 eV for Ar^+ (see Fig. 6). The sputter yield at this energy is roughly 0.25, and a high estimate for the energy carried away per atom would be 10 eV (see Ref. 46). Hence, less than 10% of the reflected energy is due to sputtered atoms, and the rest must be due to reflected energetic neutrals. At 500 eV the yield is 2.5 and the reflected energy is about 75 eV. A similar estimate would suggest that up to 30% of the reflected energy could be carried away by sputtered-gold atoms.

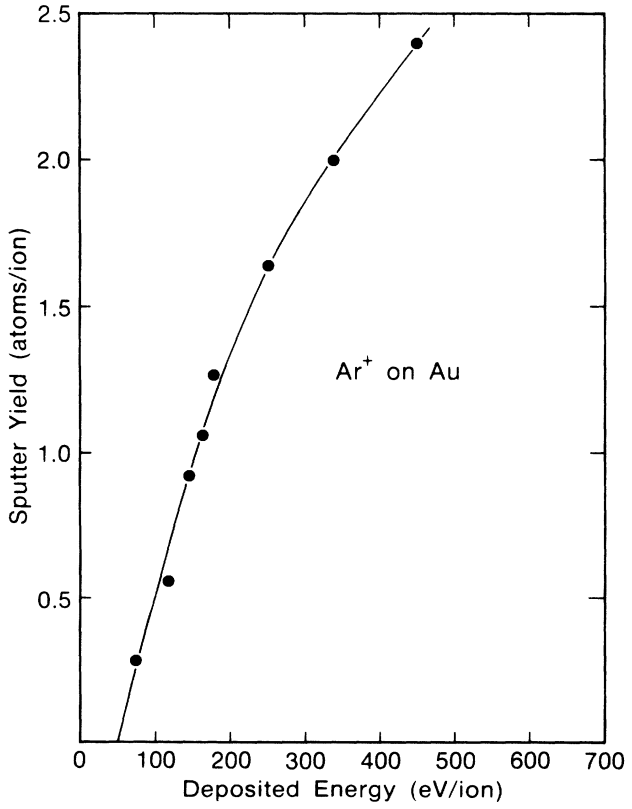

FIG. 17. Sputter yield vs deposited energy in eV/ion. Sputter yields are from Ref. 45 and the deposited energy is from Fig. 6.

E. Plasma etching

One of the major driving forces that caused the entire semiconductor industry to change from wet-chemical etching processes to plasma-assisted etching was that anisotropic profiles could be fabricated in a plasma environment.[47] The openings in the mask could be faithfully replicated without significant sideways etching occurring underneath the mask. The success of this procedure was a consequence of ion-induced chemistry. The etching reaction produced volatile products where the ions hit the surface; whereas, the reaction was very slow in other areas. However, ion-induced etching also has some deleterious consequences; e.g., damage is produced by the bombardment.[48,49] For this reason many investigators are attempting to perform ion-induced etching with very low-energy ions in order to minimize the damage. For some systems this may also have undesired consequences. Ions may hit the surface beneath the mask openings and be reflected away from the hit surface as energetic neutrals that could subsequently collide with the sidewalls. This could produce undesirable sidewall etching, as illustrated schematically in Fig. 18.

Sidewall etching would be largest when it is induced by light ions colliding with a heavy substrate. Tungsten etching in a fluorocarbon plasma is a case in point. The data of Fig. 6 suggests that as much as 40% of the energy of a CF_3^+ ion might be reflected away from the tungsten surface. It should also be remembered that the particles of a molecular ion tend to act upon the lattice independently. For example, a 400 eV CF_3^+ ion acts more like four 100 eV particles than as one 400 eV particle. The energy-reflection coefficient is larger for particles with lower energies, enhancing the possibility of undercutting

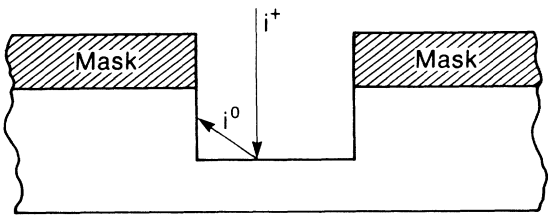

FIG. 18. Schematic diagram illustrating possible influence of reflected neutral species in plasma-assisted-etching environments.

of the mask. There are also etching reactions where the ambient environment contains hydrogen and helium.[50,51] As Fig. 6 demonstrates, a significant fraction of the kinetic energy of these light species will be reflected in collisions with solid surfaces, and it is known that energetic light ions can also give rise to significant ion-induced etching.[52] The importance of sidewall etching due to reflected energetic neutrals in a real plasma-assisted etching environment remains to be determined, but this data indicates that it would be worth investigating.

F. Sputtered thin films

In the middle 1960's, Winters and Kay[53] showed that argon was incorporated into metal films deposited by glow-discharge sputtering in a situation where there was little or no ion bombardment of the growing film. They realized that there would be no argon incorporation into the film unless energetic ($\sim$100 eV) argon particles were colliding with the surface, and therefore suggested that ions being accelerated into the target were reflected as energetic neutral-argon atoms that subsequently embedded themselves and were trapped in the growing film. It was also suggested that the number of particles and amount of energy reflected away from the target would depend upon the target mass. This is now a generally accepted picture of this phenomena even though there is no definitive evidence. Subsequently it was proposed that bombardment of the growing film by reflected energetic neutrals influences other film properties, such as stress,[54] lattice parameters,[55] the concentration of chemically active gas, etc. Data from the set of experiments will allow investigators to estimate the amount of energy reflected from the target, and thus determine whether energetic neutrals could indeed produce the phenomena attributed to them. For example, our results can be used to rationalize the observation that energetic neutrals reflected from the target produced an argon concentration of about 2 at. % in sputtered-tungsten films.[56] It is estimated that under the conditions of those experiments, reflected neutrals would have carried away from the target 10%–15 % of the incident energy and of course the fraction of particles that were reflected as energetic neutrals would necessarily have been greater than this value. Therefore the fact that 2% of them were implanted into the growing film is not unreasonable.

G. Implications for particle-spacecraft interactions

Spacecraft in low Earth orbit pass through the rarefied atmosphere in this region with velocities a little under 8 km/s. Aero-assisted orbital transfer vehicles are expected to reach about 10 km/s,[1,57] and craft returning from planetary missions might be traveling at close to 14 km/s as they encounter the first atmospheric gases.[1] Each atom or molecule will strike the craft with considerable kinetic energy at such high relative velocities, exceeding 1 eV/amu in the 14 km/s case. Figure 19 summarizes this situation, showing the range of energies most relevant to particle-spacecraft interactions for typical gases. Of particular note is the case of oxygen, which is a major component of the low Earth orbit atmosphere.

Comprehensive modeling of space flight within 100 km or so of the Earth's surface clearly requires knowledge of the energy and momentum-transfer characteristics of the individual particle-surface collisions. Drag forces on satellites, for example, depend on these momentum-transfer characteristics. A species that bounces, or is directly scattered from the satellite surface may transfer much more momentum than one that accommodates to the surface. Thus orbital lifetimes and even satellite rotation rates are determined by fine details of the scattering dynamics of a number of different species in the 1–40 eV collision energy range. Similarly, calculation of the lift-to-drag ratio for a given craft requires detailed energy and momentum transfer data, which in most cases, is not currently available. In a more extreme case, the very fate

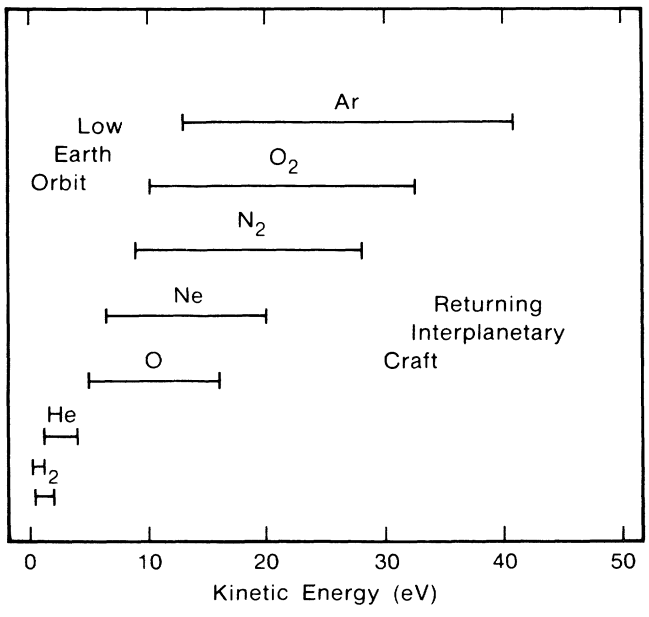

FIG. 19. Kinetic energies associated with various atomic and molecular species for velocities typical to those of spacecraft. For each species a range of energies is indicated, corresponding to relative velocities of 7.8 km/s, appropriate to craft in low Earth orbit, to 14 km/s, for returning interplanetary craft.

of a surface exposed to an atmosphere for the purpose of braking during planetary capture will depend on the microscopic atom and molecule–surface energy-transfer characteristics. If too much energy is deposited into the surface, it may simply evaporate.

Many experiments to provide the relevant parameters have been proposed and carried out, ranging from laboratory beam measurements (Refs. 1, 2, 34-38, and 57-62) to *in situ* experiments, performed on satellites[63] and even on the Shuttle.[64] However, the total amount of data obtained is rather small. This is because of the inaccessibility of the 5–20 eV region, which is too high to reach easily with supersonic neutral beams and yet so low that space-charge effects cause major problems for ion beam experiments. World-wide efforts to remedy this situation are currently underway, with an estimated 25 groups setting up O-atom generators in 1986.[1,65]

While it is beyond the scope of this paper to apply these results to space-flight problems, we believe that data such as that summarized in Fig. 16 will be of some value in this context. More importantly, we suggest that the combination of atomic- and ion-beam methods employed here may be used to provide specific results as required, possibly even for the highly relevant cases of as O atoms interacting with glasses and metal oxides.[1,2]

H. Controlled thermonuclear fusion problems

Much of the interest in the area of thermonuclear fusion is related to the collision of light ions (He, H_2, H) with a large variety of surfaces. Ito *et al.*[3] have summarized the available information by plotting the experimental data, computer-simulation data, and the predictions from a new empirical formula as functions of incident-ion energy. Reference 3 provides graphs for the projectiles *H*, *D*, *T*, ^{3}He, and ^{4}He ions incident on 40 elemental targets of atomic numbers from 3 to 92. For He^+ on gold, our values for the energy reflection coefficient, $R(E_i)$, are smaller than those empirically estimated by Ito (very roughly by a factor of 1.5 at 500 eV, 1.35 at 100 eV, and 1.25 at 10 eV). It is not clear whether or not these discrepancies are significant considering the uncertainties in the data and the estimates.

V. SUMMARY AND CONCLUSIONS

The energy deposited into evaporated, gold films by noble-gas ions has been determined for energies between 5 and 4000 eV using a novel ion-gun together with a sensitive calorimeter. We have also determined the energy loss of neutral He, Ar, and Xe atoms to a Pt(111) surface over the range 0–14 eV using supersonic atomic-beam techniques. For all energies above about 10 eV, the ions transfer at least 60% of their energy, with Xe^+ transferring the most and He^+ the least. For lower incident energies, the energy transfer from Xe remains above 60% down to the lowest energy measured ($\sim$1 eV), while for Ar and He collisions with the surface become increasingly elastic, with less than 20% and 5% energy transfer for Ar and He atoms respectively, in the low-energy limit. The effect of surface roughness on energy deposition was checked by making measurements on samples with different degrees of roughening because of ion bombardment. The fraction of kinetic energy deposited in these samples was the same within $\pm 2\%$ across the full range measured, indicating that the varying roughness produced by the ion bombardment had little effect. Similarly, we found that the observed changes in the crystallographic microstructure of the gold film produced by this treatment did not have any strong influence on the measured energy deposition.

For the neutral atoms colliding with the Pt(111) surface, the dependence of the energy lost on the angle of incidence was measured. We found that the deposited energy decreases roughly as $\cos\theta_i$, i.e., $f(\theta_i)/f(\theta_i=0°)\sim\cos\theta_i$. This simple empirical relationship can be used to predict the energy deposited into an arbitrarily rough surface for this energy range.

Consideration of the maximum energy loss in a binary collision suggests that significant lattice penetration occurs for He^+ even for energies as low as 20 eV. This conclusion is supported by evaluation of stopping power relationships, which suggest that He would need to travel over 100 Å through the lattice to account for the observed energy loss. The data is less definitive for argon and xenon but it suggests that they also penetrate the first atomic layer at close to this same energy. This data provides no evidence for breakdown of the binary-collision model for energies down to 20 eV. The data could be interpreted as indicating that this approximation breaks down at lower energies.

Comparison of this data with the sticking probability curves of Kornelsen suggests that in the low-energy range, where the sticking probabilities are small, many ions still penetrate the lattice, lose most of their energy and then diffuse back to the surface where they are subsequently desorbed into the gas phase. Our results provide a means to convert from incident energy to deposited energy for ions incident on the surface. This allowed us to reexamine earlier sputter-yield data and to address the question of proportionality between deposited energy and sputter yield. It was found that in this low-energy regime the sputter yield is not in fact strictly proportional to the energy deposited into the surface region.

The increase in reflected energy observed at low energy suggests that the use of light, low-energy ions to induce etching reactions in heavy substrates may produce unwanted undercutting of the mask. Comparison of this data with measurements of the noble-gas concentration in sputtered films indicates that the interpretation of those measurements in terms of the entrapment of energetic, reflected neutrals from the target is probably correct.

ACKNOWLEDGMENTS

The authors gratefully acknowledge the very capable technical assistance of Dean Pearson, Joe Schlaegel, and Robert Grygier. We also thank John Duran for providing SEM micrographs, Grace Gorman for x-ray diffraction measurements, and Dolores Miller for electron spectroscopy for chemical analysis (ESCA) studies.

[1]F. C. Hurlbut, Prog. Astronaut. Aeronaut. **116**, 419 (1989).
[2]F. C. Hurlbut, in *Thermophysical Aspects of Reentry Flows* (American Institute of Astronautics and Aeronautics, New York, 1986).
[3]R. Ito, T. Tabata, N. Itoh, K. Morita, T. Kato, and H. Tawara, The Institute of Plasma Physics, Report No. IPPJ-AM-41, 1985 (unpublished).
[4]D. Hildebrandt and R. Manns, Phys. Status Solidi A **38**, K155 (1976).
[5]J. Schou, H. Sorensen, and U. Littmark, J. Nucl. Mater. **76**, 389 (1978).
[6]H. H. Andersen, T. Lenskjaer, G. Sidenius, and H. Sorensen, J. Appl. Phys. **47**, 13 (1976).
[7]N. N. Koborov, V. A. Kurnaev, V. G. Telkovsky, and G. I. Zhabrev, Radiat. Eff. **69**, 135 (1983).
[8]H. H. Andersen, Radiat. Eff. **3**, 51 (1970).
[9]H. H. Andersen Radiat. Eff. **7**, 179 (1971).
[10]P. Sigmund, Can. J. Phys. **46**, 731 (1968).
[11]W. Eckstein and J. P. Biersack, Z. Phys. A **310**, 1 (1986).
[12]W. Eckstein and J. P. Biersack, Z. Phys. B **63**, 471 (1986).
[13]O. S. Oen and M. T. Robinson, Nucl. Instrum Methods **132**, 647 (1976).
[14]H. F. Winters and D. Horne, Phys. Rev. B **10**, 55 (1974).
[15]W. R. Gesang, H. Oechsner, and H. Schoof, Nucl. Instrum. Methods **132**, 687 (1976).
[16]W. Eckstein and H. Verbeek, Max-Planck-Institute of Plasma Physics Report No. IPP 9/32, 1979 (unpublished).
[17]H. Sorensen, Appl. Phys. Lett. **29**, 148 (1976).
[18]H. Coufal, R. K. Grygier, D. Horne, and J. E. Fromm, J. Vac. Sci. Technol. **5**, 2875 (1987).
[19]C. T. Rettner, L. A. DeLouise, and D. J. Auerbach, J. Chem. Phys. **85**, 1131 (1986).
[20]E_e terms are estimated assuming secondary electron emission below about 500 eV to be dominated by potential emission. See, for example H. D. Hagstrum, Phys. Rev. **96**, 336 (1959); **104**, 672 (1956); **122**, 83 (1961); H. D. Hagstrum, Y. Takeishi, and D. P. Pretzer, *ibid.* **139** A526 (1965). We therefore expect it to have a similar energy dependence and absolute value for many materials.
[21]D. N. Ruzic and H. K. Chiu, J. Nucl Mater. **16**, 904 (1989).
[22]See, for example, J. Anderson, in *Molecular Beams and Low Density Gas Dynamics,* edited by P. P. Wegener (Dekker, New York, 1974), p. 1.
[23]J. E. Hurst, L. Wharton, K. C. Janda, and D. J. Auerbach, J. Chem. Phys. **78**, 1559 (1983).
[24]H. D. Hagstrum, Phys. Rev. **150**, 495 (1966), p. 505.
[25]M. T. Robinson and I. M. Torrens, Phys. Rev. B **9**, 5008 (1974).
[26]G. Carter and J. S. Colligon, *Ion Bombardment of Solids* (Elsevier, New York, 1968), p. 33.
[27]U. A. Arifov, *Interaction of Atomic Particles with the Surface of a Metal* (Tashkent University, Uzbekhisstau, 1961) [English translation in Atomic Energy Commission Report No. AEC-Tr 6089 (unpublished).
[28]L. G. Gurvich, Izv. Akad. Naak. S. S. R. **26**, 1418 (1962).
[29]J. P. Biersack and W. Eckstein, Appl. Phys. **34**, 73 (1984); W. Eckstein and J. P. Biersack, Z. Phys. B **63**, 471 (1986), see Fig. 2, noting that 1000 eV is equivalent to a reduced energy of 4.2×10^{-2}, 3.4×10^{-3}, and 7.1×10^{-4}, for He, Ar, and Xe colliding with Au.
[30]F. O. Goodman and H. Y. Wachmann, *Dynamics of Gas-Surface Scattering* (Academic, New York, 1976).
[31]W. H. Weinberg and R. P. Merrill, J. Vac. Sci. Technol. **8**, 718 (1971).
[32]E. K. Grimmelmann, J. C. Tully, and M. J. Cardillo, J. Chem. Phys. **72**, 1039 (1980).
[33]P. Loftager, F. Besenbacker, O. S. Jensen, and V. S. Sorenson, Phys. Rev. A **20**, 1443 (1979).
[34]R. A. Oman, J. Chem. Phys. **48**, 3919 (1968).
[35]D. R. Miller and R. B. Subbarao, J. Chem. Phys. **52**, 425 (1970).
[36]S. M. Lui, W. E. Rodgers and E. L. Knuth, *Proceedings of the Ninth International Symposium on Rarefied Gas Dynamics* (DFVLR, Porz-Wahn, 1974), Vol. II, p. E.8-1.
[37]A. Amirav, M. J. Cardillo, P. L. Trevor, C. Lim, and J. C. Tully, J. Chem. Phys. **87**, 1796 (1987).
[38]C. T. Rettner and E. K. Schweizer, Surf. Sci. **203**, L677 (1988).
[39]P. Sigmund, Phys. Rev. **184**, 383 (1969).
[40]J. Lindhard, J. Nielsen, and M. Schaff, Mat. Fys. Medd. Dan. Vid. Selsk. **36**, 10 (1968).
[41]G. Carter and J. S. Colligon, *Ion Bombardment of Solids* (Elseveir, New York, 1968), p. 100.
[42]E. V. Kornelsen and M. K. Sinha, J. Appl. Phys. **40**, 2888 (1969).
[43]K. J. Close and J. Yarwood, Br. J. Appl. Phys. **18**, 1593 (1967).
[44]E. V. Kornelsen, F. Brown, J. A. Davies, B. Domeij, and G. R. Piercy, Phys. Rev. A **136**, 849 (1964).
[45]G. K. Wehner, General Mills Report No. 2309, 1962 (unpublished).
[46]R. V. Stuart and G. K. Wehner, J. Appl. Phys. **35**, 1819 (1964).
[47]J. W. Coburn and H. F. Winters, Annu. Rev. Mater. Sci. **13**, 91 (1983).
[48]J. M. Heddleson, M. W. Horn, and S. J. Fonash, J. Vac. Sci. Technol. B **6**, 280 (1988).
[49]S. W. Pang, M. W. Geis, N. N. Efremow, and G. A. Lincoln, J. Vac. Sci. Technol. B **3**, 398 (1985).
[50]L. M. Ephrath and J. Petrillo, J. Electrochem. Soc. **129**, 2282 (1982).
[51]C. M. Knoedler, L. Osterling, and H. Shtrikman, J. Vac. Sci. Technol. B **6**, 1573 (1988).
[52]U. Gerlach-Meyer, J. W. Coburn, and E. Kay, Surf. Sci. **103**, 177 (1981).
[53]H. F. Winters and E. Kay, J. Appl. Phys. **38**, 3928 (1967).
[54]J. A. Thornton and D. W. Hoffman, J. Vac. Sci. Technol. A **3**, 576 (1985).
[55]E. Kay, F. Pamigiani, and W. Parrish, J. Vac. Sci. Technol. A **5**, 44 (1987).
[56]H. F. Winters and E. Kay, J. Appl. Phys. **43**, 794 (1972).
[57]G. D. Walberg, J. Spacecr. Rockets **22**, 3 (1985).
[58]F. M. Devienne, J. Souquet, J. G. Roustan, in *Proceedings of the 4th International Symposium on Rarefied Gas Dynamics, 1966,* edited by J. H. de Leeuw (Academic, New York, 1966), Vol. II, p. 384.
[59]E. D. Knechtel and W. C. Pitts, in *Proceedings of the 6th International Symposium on Rarefied Gas Dynamics, 1969,* edited by L. Trilling and H. Watchman (Academic, New York, 1969), Vol. II, p. 1257.
[60]E. Hulpke and K. Mann, Surf. Sci. **133**, 171 (1983).
[61]E. Kolodney, A. Amirav, R. Elber, and R. B. Gerber, Chem. Phys. Lett. **113**, 303 (1985).
[62]A. D. Tenner, K. T. Gillen, T. C. M. Horn, J. Los, and A. W. Kleyn, Phys. Rev. Lett. **52**, 2183 (1984); Surf. Sci. **172**, 121 (1986).
[63]E. N. Evlanov and Yu. V. Lebedev, in *Proceedings of the 9th International Symposium on Rarefied Gas Dynamics, 1974,* edited by M. Becker and M. Fiebig (DFVLR, Linder Höhe,

1974), Vol. II, p. E-16.

[64]S. J. Gregory and R. N. Peters, in *Proceedings of the 15th International Symposium on Rarefied Gas Dynamics, 1986*, edited by V. Boffi, C. Cercignani, and R. G. Teubner (Academic, New York, 1986), Vol. I, p. 644.

[65]See, *Proceedings of the NASA Workshop on Atomic Oxygen Effects, Pasadena, 1987*, edited by D. E. Brinza (JPL, Pasadena, 1987).

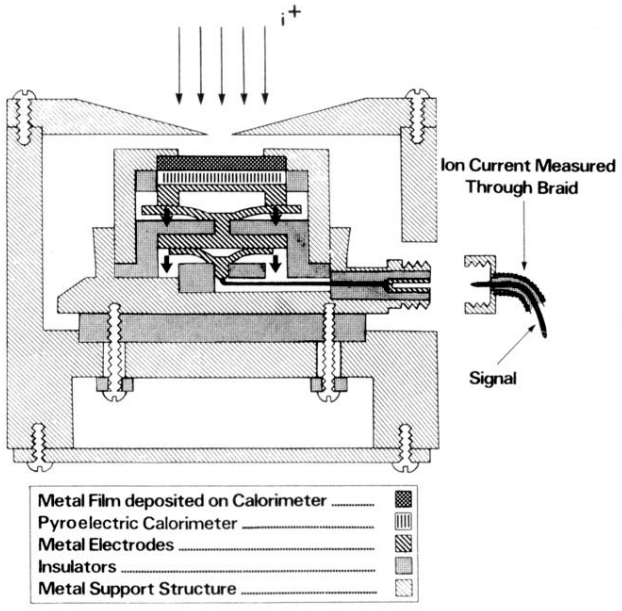

FIG. 1. Pyroelectric calorimeter. The modulated-ion beams bombard the grounded front surface of the calorimeter through a 3.2-mm-diam aperture. The signal goes from the back electrode through two spring contacts (indicated by arrows) to a lockin detector.

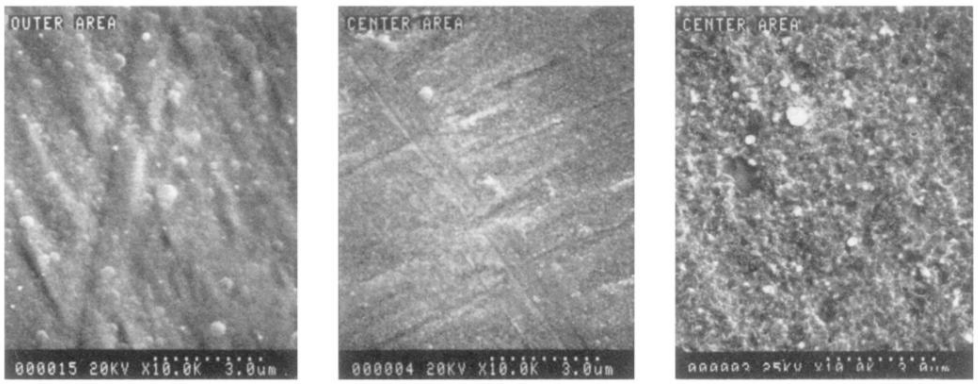

FIG. 8. Scanning electron micrograph of the gold surface. (a) Unbombarded area. (b) Lightly bombarded sample. (c) Heavily bombarded sample used in most of these experiments. The white dots indicate a length of 3 μm.